Br J Dermatol 2026; **194**:737–746
https://doi.org/10.1093/bjd/ljaf516
Advance access publication date: 10 December 2025

BJD
British Journal of Dermatology
Translational Research

Automated classification of site-specific cutaneous photodamage using a convolutional neural network and three-dimensional total body photography

Sam Kahler,[1] Siyuan Yan,[2] Adam Mothershaw,[1,3] Francesco Leo,[1] Chantal Rutjes,[1] Zhen Yu,[2] Dilki Jayasinghe,[3] Victoria Mar,[5] Monika Janda,[3] Zongyuan Ge,[2] H Peter Soyer,[1,4] Brigid Betz-Stablein[1] and Clare A Primiero[1]

[1]Frazer Institute, The University of Queensland, Dermatology Research Centre, Brisbane, QLD, Australia
[2]Electrical and Computer Systems Engineering, Faculty of Engineering, Monash University, Melbourne, VIC, Australia
[3]Centre for Health Services Research, Faculty of Medicine, The University of Queensland, Brisbane, QLD, Australia
[4]Dermatology Department, Princess Alexandra Hospital, Brisbane, QLD, Australia
[5]Victorian Melanoma Service, Alfred Hospital, Melbourne, VIC, Australia

Correspondence: Clare Primiero. Email: c.bover@uq.edu.au

Abstract

Background Early detection of melanoma presents a major public health challenge. Growing evidence supports targeted surveillance of individuals at high risk identified using risk stratification. Skin photodamage is the primary environmental risk factor for melanoma; however, it is inconsistently captured and often relies on self-reporting or subjective observations, resulting in poor reproducibility. The increasing use of total-body photography (TBP) in clinical skin examinations, combined with advances in artificial intelligence technology, presents new opportunities for automated skin assessment of ultraviolet damage.

Objectives To develop a clinical photonumeric scale for photodamage assessment, use the scale to build a dataset of annotated image tiles, and train a convolutional neural network (CNN) to automate photodamage assessment from three-dimensional (3D) TBP.

Methods Our photonumeric scale was validated for assessing photodamage and pigmentation from 3D TBP by comparing inter-rater reproducibility between two dermatology research students and two lay people. A total of 24 720 cutaneous image tiles from 56 individuals at high risk and 51 at population risk for melanoma were annotated. Annotated images were used to train a CNN with a multi-task learning (MTL) strategy that incorporated pigmentation as an auxiliary task to increase the performance for photodamage. The MTL-CNN was compared with a single-task CNN that considered photodamage in isolation.

Results Lay people achieved substantial-to-almost perfect agreement with dermatology research students using the photonumeric scale ($\kappa = 0.77–0.83$). The MTL-CNN design improved performance compared with the single-task CNN, with receiver operating characteristic area under the curve (ROC-AUC) increasing from 0.91 to 0.96 ($P < 0.01$). Class-specific accuracy improved for mild (0.96 to 0.98; $P = 0.04$), moderate (0.85 to 0.92; $P < 0.01$) and severe (0.97 to 0.99; $P < 0.01$) photodamage categories, and was maintained across each body site (range 0.86–0.92). Accuracy was reproduced in an external validation set with a ROC-AUC of 0.93, including class-specific accuracies of 0.97 for mild, 0.85 for moderate and 0.97 for severe photodamage. An interface was developed to display CNN-labelled photodamage as heatmaps on 3D TBP patient avatars for clinical interpretation.

Conclusions Our CNN provides a novel tool to automatically and reproducibly report an individual's photodamage phenotype from 3D TBP. Incorporating this assessment into risk prediction models may inform targeted risk prediction facilitating surveillance recommendations.

Accepted: 8 December 2025

Lay summary

Sun damage to the skin is the main environmental risk factor for melanoma. However, current risk assessment tools rarely use sun damage as there is no simple or reliable way to measure it across the whole body. Current methods usually need people to report past sun exposure. This includes how much time they spent outdoors or how many severe sunburns they had as a child. Such estimates are often unreliable because they depend on memory. To address this difficulty, we developed a visual scale to help assess sun damage on skin. The study took place in Australia.

We tested how reliable the scale was. We compared how clinicians and lay people rated the same skin images. We found high similarity of rating. We then recruited the lay people to assess ('label') a large dataset of skin images (24,750 image tiles). This dataset was made from photos using a special three-dimensional (3D) body scanner that uses 2D skin photos to create a 3D map ('avatar') of a person. The dataset included photos from 107 volunteers. From each volunteer, over 200 image tiles were collected for the dataset. The labelled image tiles were then used to 'train' an artificial intelligence (AI) system to automatically detect sun damage.

The AI system reported sun damage with very high accuracy. It performed better when trained to recognize both sun damage and skin pigmentation, versus sun damage alone. We also carried out 'external validation' of the AI system. This means we tested it using images from a group of people not part of the original set. The AI results are shown using colour-coded areas on the 3D human avatars ('heatmaps'). These show areas of mild, moderate or severe sun damage.

Overall, we showed our AI system provides an automated way to measure sun damage across the entire body using 3D total-body photography. This tool could be used to improve skin cancer risk assessment and guide more personalized skin cancer screening.

What is already known about this topic?

- Ultraviolet exposure is the primary environmental risk factor for cutaneous melanoma.
- Clinical risk prediction tools for melanoma that consider photodamage often rely on self-reporting and subjective assessment that is prone to recall bias and poor reproducibility.
- Parallel advances in three-dimensional total-body photography (3D TBP) and artificial intelligence present new opportunities for automated assessment of cutaneous phenotypes.

What does this study add?

- We present a convolutional neural network (CNN) for automatic evaluation of site-specific photodamage using 3D TBD.
- To increase clinical utility, we developed a user interface where photodamage is presented as heatmaps on 3D avatars.
- Training a CNN on photodamage and pigmentation simultaneously within a multi-task learning strategy improves the predictive performance for photodamage.
- We developed a photonumeric scale to enable reproducible annotation of cutaneous photodamage and pigmentation by lay people.

What is the translational message?

- Our CNN allows for the automatic assessment of whole-body skin photodamage directly from 3D TBD that is increasingly used in clinical melanoma surveillance.
- The automatic assessment of skin photodamage may be interpreted by the clinician performing surveillance, or incorporated into risk prediction models to assist with personalized, targeted methods for the earlier detection of melanoma.

Ultraviolet (UV) radiation is the primary environmental risk factor in the tumorigenesis of melanoma.[1] Chronic exposure with intermittent sunburns results in distinct histopathological changes of dermal elastosis and epidermal atrophy that can be visually approximated as photodamage.[2] Melanocytes at sites with chronic or intermittent UV exposure demonstrate a stepwise increase in tumour mutational burden (TMB) compared with nonexposed melanocytes.[3] Quantifying photodamage as a surrogate of the UV-induced TMB offers a personalized measure for melanoma risk.[4]

However, the challenge of accurate and feasible measurement means that photodamage is rarely included in risk prediction models.[5] A recent systematic review of risk prediction models reported the use of five surrogate measures of sun damage (sunburns, sunbed use, sun exposure, occupational sun exposure and use of sunscreen) as risk factors.[6] Models that incorporated sun damage were limited to a single body site measurement that was used to assume a whole-body distribution.[6] Existing photonumeric scales to aid photodamage assessment are limited to the face[7] and forearm,[8] rather than considering total and site-specific patterns.[9] However, even when used by a clinician, reproducible assessment of photodamage is susceptible to inter-rater variability.[10] An automated assessment of photodamage by severity and body site distribution would provide enhanced

capacity to identify the burden of UV-associated damage and subsequent risk of melanoma tumorigenesis.

The integration of artificial intelligence (AI) with three-dimensional total-body photography (3D TBP) facilitates the automated and reproducible assessment of cutaneous phenotypes.[9] 3D TBP is increasingly recommended by clinical guidelines to monitor individuals at high risk for melanoma, providing a detailed record of the entire skin surface phenotype.[11–13] The deep imaging phenotype concept in dermatology describes leveraging AI algorithms to measure the severity and spatial distribution of cutaneous risk factors directly from TBP.[9,14] To date, most algorithms in dermatology have focused on single lesions and have been criticized for their experimental nature; such methods fail to replicate the complexities of real-world clinical examinations.[15,16] A whole-of-patient approach is proposed to provide a more holistic assessment, whereby suspicious lesions would be considered in the context of the surrounding skin and an individual's risk for malignancy.[13,17]

The aim of this study was to utilize 3D TBP images integrated with AI to facilitate an automated and reproducible assessment of site-specific skin photodamage, thereby enhancing melanoma risk assessment and diagnosis.

Materials and methods

Study design

The 3D TBP avatars were selected from two clinical studies conducted in Queensland, Australia.[18,19] The first study recruited people from the general population; the second targeted high-risk individuals. Eligibility criteria for general population individuals were age 18 years or older, and at least one mole. Eligibility criteria for high-risk individuals were as follows: (i) at least one melanoma (including *in situ*) diagnosed before the age of 40 years; (ii) two or more melanomas (including *in situ*) diagnosed before the age of 65; and (iii) a strong family history (two or more first-degree relatives affected) and/or known pathogenic mutations in a hereditary melanoma gene and/or a diagnosis of dysplastic naevus syndrome.[19]

3D TBP was conducted for all participants, using a VECTRA WB360 whole body 3D imaging system (Canfield Scientific Inc., Parsippany, NJ, USA), which instantaneously captures 92 cross-polarized 2D images with standardized stance, camera angles and lighting, and subsequently merges them to create a 3D avatar. A subset of high-risk ($n=56$) and population-risk ($n=51$) avatars were included for annotation (Table S1; see Supporting Information). Targeted selection of individuals was used to achieve balanced representation of mild, moderate and severe phenotypes. Specifically, the first 50% of individuals within high-risk and population-based groups were randomly selected, while the remaining 50% were randomly selected from the subset of individuals previously noted to have moderate-to-severe photodamage (vs. none-to-mild) during clinical review.

'Image tiles' (each 693×693 pixels) were created from the original 92 raw 2D images, representing approximately 10 cm^2 of cutaneous surface. Pixel colour analysis was used to exclude image tiles with < 33% skin surface, and the remainder were manually reviewed to exclude image tiles that were out of focus, contained multiple body sites, or included identifying features such as tattoos or facial regions (Figure S1; see Supporting Information). Minor differences in image curvature due to camera positioning was accepted. The yield from each individual comprised approximately 2000 image tiles, of which half were removed by pixel detection, and up to 800 removed by manual inspection, to yield 200–600 image tiles per participant.

Photonumeric scale development

Representative image tiles of mild, moderate and severe photodamage were chosen by a dermatology-trained PhD student/clinician (S.K.) and senior dermatologist (H.P.S.). These phenotypes varied based on background pigmentation, specifically the disposition of lighter phototypes for hypertrophic and darker phototypes for atrophic histological photodamage.[20] For this reason, examples of nine distinct phenotypes were selected to form a clinical photonumeric scale of increasing photodamage. The scale was formalized in mirrored colour and greyscale formats to aid evaluation of photodamage and, as an auxiliary task, pigmentation [Figure 1, Figure S2 (see Supporting Information)]. Specific cutaneous features used to discriminate photodamage-pigmentation phenotypes are listed in Table S2 (see Supporting Information).

Photonumeric scale validation

Reproducibility of the photonumeric scale was evaluated comparing annotations by two dermatological research students (S.K., C.R.) and two lay people employed through the ethical crowd-sourcing platform Isahit (Paris, France). Student annotators completed overlapping annotation of 6195 image tiles. An inter-rater validation dataset was created, comprising 100 image tiles including 11 image tiles of each photodamage-pigmentation phenotype derived from the student consensus. This validation dataset was used for inter-rater validation alone and excluded from CNN design. Emphasis was placed on achieving agreement between photodamage annotations, with pigmentation included to support this objective.

Image annotation

Prior to external annotation by the lay people through Isahit, we provided a training video outlining application of the photonumeric scale, including exclusion of noncontributory cutaneous findings such as varicose veins (Video S1; see Supporting Information). Isahit lay people were required to complete a practice set of 27 images with 80% correct responses, prior to labelling the total image dataset of 13 386 images.

Convolutional neural network model development

Convolutional neural network dataset

The training dataset included 13 386 images annotated by laypersons, and 11 689 images annotated by dermatology students. The validation ($n=1019$) and test ($n=1019$)

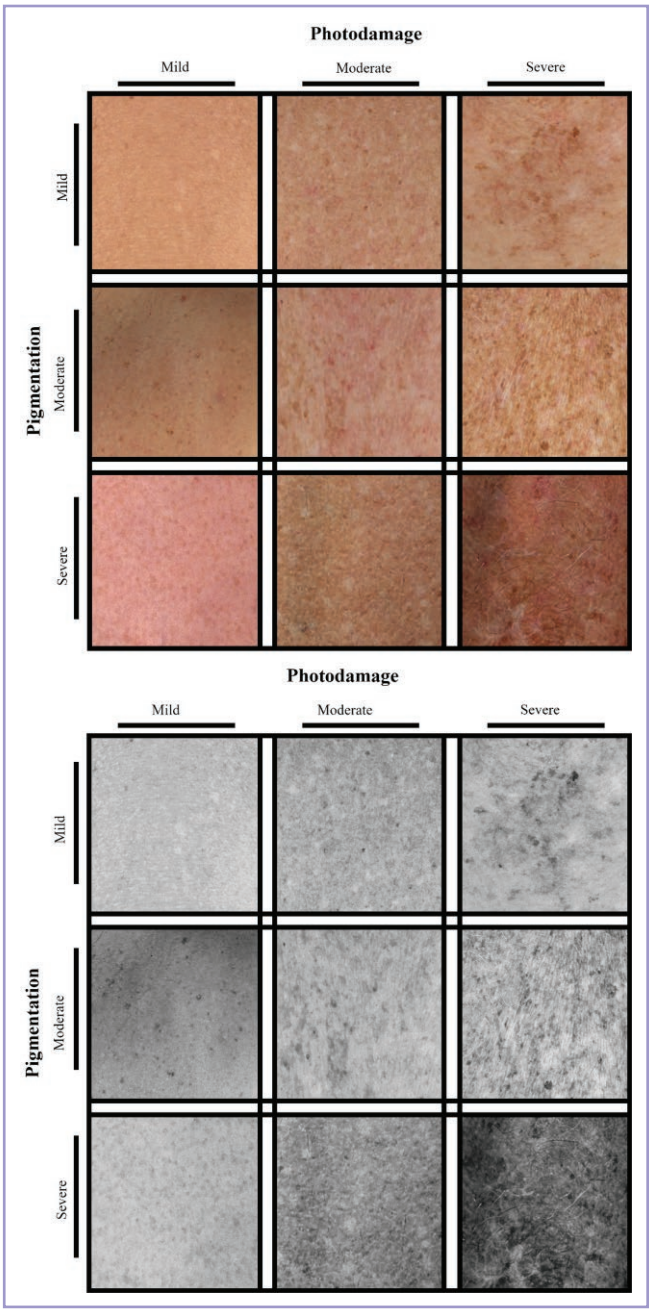

Figure 1 Photonumeric scale demonstrating increasing photodamage (*x*-axis) and pigmentation (*y*-axis) to define three photodamage phenotypes, with a specific image for each level of pigmentation within the photodamage class (colour and greyscale).

datasets included only annotation by dermatology students. A convolutional neural network (CNN) was designed to assess photodamage from image tiles. Specifically, a transfer learning strategy was developed employing the pretrained ResNet50[21] model with ImageNet[22] pretrained weights, and was fine-tuned on our training set. Input image tiles underwent data augmentation strategies to increase the variety, and improve model robustness.[23] Specifically, all image tiles underwent resizing to 256×256 resolution, random cropping to 224×224 resolution, random horizontal flipping and random vertical flipping. Individuals were randomly allocated to either the training, validation or test datasets, with all image tiles from a single individual featuring within only one dataset to ensure independence. An imbalanced class problem was identified with over-representation of moderate image tiles. Therefore, weighted random sampling was used to oversample under-represented mild and severe image tiles to balance the class distribution.

The CNN was fine-tuned using a multi-task learning strategy (MTL) that introduced an auxiliary prediction branch for the pigmentation phenotype (Figure 2a–f). Incorporating pigmentation as an auxiliary task acted to regularize model training and improve the photodamage prediction performance. Specifically, the shared optimization layer forces the algorithm to learn features that generalize across both tasks, preventing the model from overfitting to spurious patterns in the photodamage labels, and from over-interpreting pigmentation-related variation as photodamage. The model was implemented using a minibatch size of 100, learning rate of $3e^{-4}$, and weight decay of $1e^{-4}$. Training was conducted on a single GeForce RTX 3090 GPU (NVIDIA, Santa Clara, CA, USA) using the Adam optimizer for 20 epochs, with early stopping set to a patience of 5. The model converged efficiently with cross-entropy loss decreasing from 0.75 to 0.45 within 4 epochs and remaining stable thereafter (Figure S3; see Supporting Information). The optimal model was selected based on the cross-entropy loss on the validation set.

Convolutional neural network model evaluation

External validation

The model was evaluated on an external test set that was contributed by an external institution (Monash University, Victoria). 3D TBP images of 25 individuals were randomly selected from a surveillance cohort at high risk for melanoma. 3D TBP images were prepared as image tiles (n=4980), and annotations of the CNN and a dermatology clinician were compared with each other.

Quantitative metrics

The model was trained with five random seeds, and accuracy recorded using means and SDs. The final MTL-CNN model was compared with a CNN that considered photodamage in isolation, to quantify the performance improvement achieved by integrating pigmentation as an auxiliary task.

Qualitative metrics

Annotated image tiles were reconstructed into avatars to visualize photodamage distributions. The site-specific severity within each body region was calculated based on the MTL-CNN assessment of the combined training, test and validation datasets to ensure whole-body coverage, with grey areas representing insufficient image tiles due to clothing or image quality. The head region was excluded to anonymize data. The surface area of severe, moderate and mild photodamage was extracted from heatmaps to quantitatively assess CNN output.

Statistical analysis

Descriptive statistics were used to summarize participant characteristics alongside χ^2 (parametric) and Fisher's exact

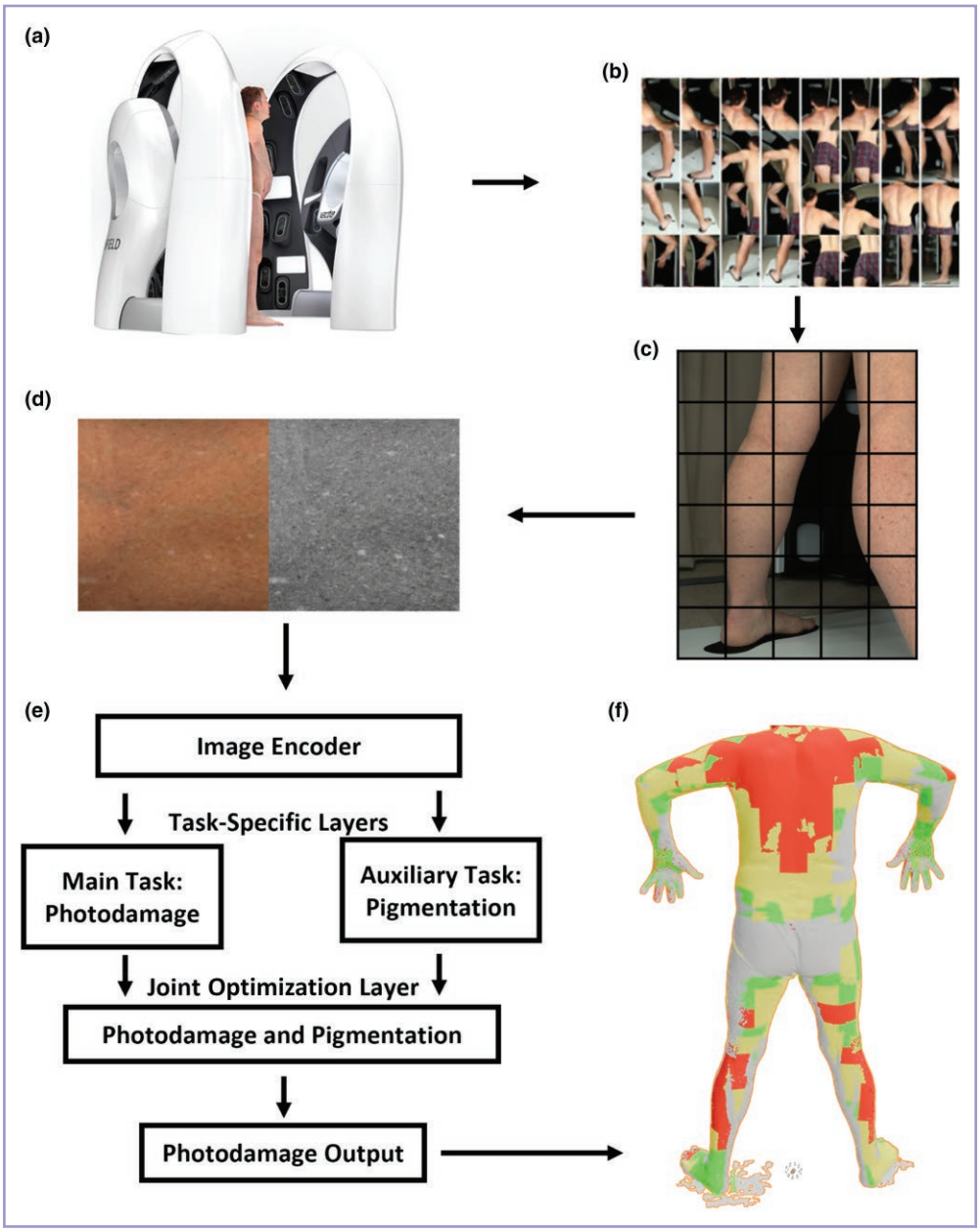

Figure 2 Overview of image processing and the multi-task learning convolutional neural network. (a) Three-dimensional (3D) total-body photography images were taken using the Vectra WB360 (Canfield Scientific Inc., Parsippany, NJ, USA). (b) Raw 2D images were extracted and referenced to the specific body site. (c) 'Image tiles' were created representing approximately 10 cm^2 of cutaneous surface. (d) The photonumeric scale was developed to objectively label image tiles for photodamage and pigmentation. (e) Image tiles were processed using a ResNet50 image encoder with the main task predictor for photodamage, and an auxiliary task predictor for pigmentation. (f) 'Image tiles' labelled for photodamage were reconstructed onto 3D avatars to present the pattern and severity of photodamage for clinical interpretation.

(nonparametric) tests to evaluate for differences. A statistical significance threshold of $P<0.05$ was used. Agreement was evaluated using Cohen's quadratic weighted kappa (κ). Analysis was conducted in R version 3.4.1.[24]

Results

Study population

Participant image tile datasets included 56 individuals at high risk and 51 at population risk for melanoma (Table S1). Both high- and population-risk profiles were included to create a generalizable CNN and prevent overfitting. The median age of participants was 63 years (range 53–68) with 57% male. Most participants (86%) were born in Australia, with British or Irish ancestry (88%). Compared with population-risk individuals, high-risk participants were older (mean age 66 years vs. 50 years; $P<0.001$), with a higher proportion having British or Irish ancestry (98% vs. 76%; $P=0.002$). High-risk participants had a greater burden of melanoma history, including 47 (84%) with multiple melanomas and 9 (16%) with a single diagnosis, compared with the population-risk group, which included 3 (6%) with a single diagnosis and

48 (94%) without melanoma history ($P<0.001$). Similarly, high-risk individuals had a higher burden of nonmelanoma skin cancer (91% vs. 15%; $P<0.001$).

Validation of the photonumeric scale

The clinical photonumeric scale was developed to facilitate the reproducible annotation of photodamage (Figure 1; Figures S1, S2). Students annotated an overlapping database of 6195 image tiles with weighted κ demonstrating almost perfect photodamage inter-rater reliability [$\kappa=0.81$, 95% confidence interval (CI) 0.79–0.82] (Table S3; see Supporting Information).

The two lay person annotators demonstrated almost perfect ($\kappa=0.83$, 95% CI 0.76–0.90) to substantial agreement ($\kappa=0.77$, 95% CI 0.68–0.85), respectively, compared with students, and substantial agreement ($\kappa=0.73$, 95% CI 0.64–0.82) compared with one another, when evaluating the inter-rater validation dataset (comprising 100 image tiles with random class-balanced selection).

Pigmentation, evaluated as an auxiliary task (Table S4), using the same dataset demonstrated moderate inter-rater reliability between student annotators ($\kappa=0.51$, 95% CI 0.49–0.53), fair agreement between students and respective lay people ($\kappa=0.32$, 95% CI 0.15–0.49 and $\kappa=0.23$, 95% CI 0.06–0.40) and substantial agreement between lay people ($\kappa=0.79$, 95% CI 0.69–0.90).

Data annotation

Annotators labelled a total of 24 720 image tiles, including 16 845 from high-risk and 7875 from general population-risk participants (Table S5; see Supporting Information). Among the image tiles, the distribution of photodamage was mild in 36% (8667), moderate in 42% (10 292) and severe in 23% (5761). The distribution of pigmentation was mild in 35% (11 472), moderate in 46% (8618) and severe in 18% (4559).

Convolutional neural network performance

The baseline CNN (photodamage only) achieved a high prediction performance with receiver operating characteristic area under the curve (ROC-AUC) of 0.91 (95% CI 0.90–0.93) compared with ground truth annotations (Figure 3a). The class-specific accuracy for mild photodamage was 0.96 (95% CI 0.95–0.98), for moderate was 0.85 (95% CI 0.83–0.88) and for severe was 0.97 (95% CI 0.95–0.98).

When pigmentation was integrated into the model, the MTL-CNN achieved an increase in the AUC from 0.91 to 0.96 (95% CI 0.95–0.98) (Figure 3b). Class-specific accuracy demonstrated relevant improvements in the capacity to accurately classify moderate photodamage (from 0.85 to 0.92, 95% CI 0.91–0.94; $P<0.01$), as well as improvements in mild (from 0.96 to 0.98, 95% CI 0.97–0.99; $P=0.04$) and severe photodamage (from 0.97 to 0.99, 95% CI 0.98–1.00; $P=0.02$).

The MTL-CNN maintained strong performance on an external validation set, achieving an accuracy of 0.93 (95% CI 0.92–0.95) (Figure 3c). The class-specific accuracies were 0.97 (95% CI 0.96–0.99) for mild, 0.85 (95% CI 0.82–0.87) for moderate and 0.97 (95% CI 0.95–0.98) for severe photodamage. This accuracy was maintained across all body sites including the anterior torso (0.92, 95% CI 0.91–0.94), posterior torso (0.91, 95% CI 0.89–0.92), upper limb (0.86, 95% CI 0.83–0.89) and lower limb (0.89, 95% CI 0.88–0.91) (Figure 3d).

Reconstructed heatmaps for site-specific phenotype

To increase clinical utility of the CNN output, the severity and site-specific distribution of photodamage can be viewed as heatmaps overlaid on an individual's 3D TBP avatar (Figure 4). The use of different colours to represent photodamage as mild (green), moderate (yellow) and severe (red), provides an efficient report for personalized assessment of the photodamage phenotype. Figure 4 illustrates four observed phenotype patterns comprising predominantly: total-body low, moderate or severe photodamage, or a mixed photodamage severity phenotype. The surface area affected by each photodamage severity was extracted as a quantifiable metric to accompany the heatmaps. This demonstrates the importance of a site-specific phenotypic assessment.

Discussion

Our CNN demonstrates that site-specific photodamage can be automatically and accurately measured from total-body photography images. Classification of mild, moderate or severe photodamage can be reported by body site, or reconstructed onto 3D TBP avatars as a visual heatmap interface to visualize the CNN output across the total skin surface. To our knowledge, this is the first reported AI model for automatic assessment of photodamage from TBP. Implementation of this technology is broadly relevant for skin cancer risk stratification. Photodamage may serve as the principal phenotypic risk factor for keratinocyte cancers, while melanoma risk prediction will benefit from integration with other phenotypic risk factors, including naevus count and distribution.

The high variability in the anatomical severity and distribution of photodamage posits that site-specific evaluation is essential.[25] Variability in photodamage across body sites has been reported in Australian,[25] North American[26] and European populations,[27] and probably varies further across other geographic regions. The cumulative photodamage burden is reported to be higher in Australian populations compared with those of North America and Europe, largely attributed to the intensity of UV exposure, lifestyle, culture, and a high proportion of the population with fair skin.[26,28] Photodamage assessed at a single site is unlikely to accurately capture an individual's total burden of UV exposure, and could not only lead to flawed risk assessment but also potentially generate misleading associations between photodamage and cutaneous malignancies.[3,25,27]

The major strength of our CNN model is the quality of the training dataset. This was achieved by firstly developing a reliable photonumeric scale that lay people could be instructed to use with high accuracy. Validation steps provided evidence on the usability of the scale, showing excellent-to-good agreement between annotators. A final

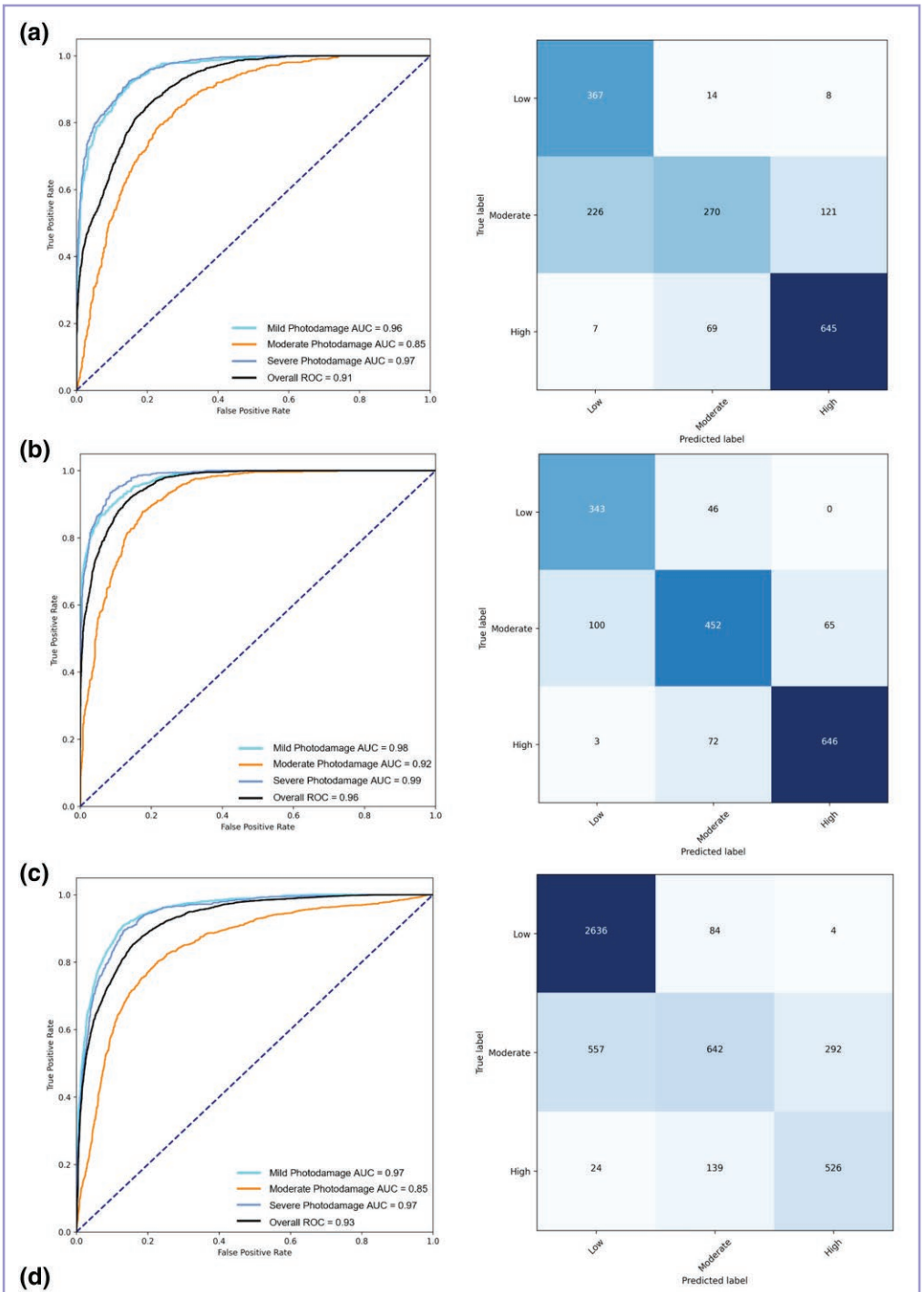

Body Region	Accuracy (95% CI)	Mild *n* (%) at site	Moderate *n* (%) at site	Severe *n* (%) at site
Anterior Torso	0.92 (0.91–0.94)	534 (49%)	296 (27%)	271 (25%)
Posterior Torso	0.91 (0.89–0.92)	424 (33%)	490 (38%)	390 (30%)
Upper Limbs	0.86 (0.83–0.89)	168 (27%)	172 (28%)	271 (44%)
Lower Limbs	0.89 (0.88–0.91)	889 (55%)	323 (20%)	419 (26%)

Figure 3 Performance using receiver operating characteristic (ROC) area under the curve (AUC) and confusion matrices for convolutional neural network (CNN) algorithms. (a) Baseline CNN using photodamage in isolation; (b) multi-task learning (MTL)-CNN using photodamage and pigmentation; (c) external validation MTL-CNN; and (d) prediction accuracy at specific body regions on the external validation dataset. CI, confidence interval.

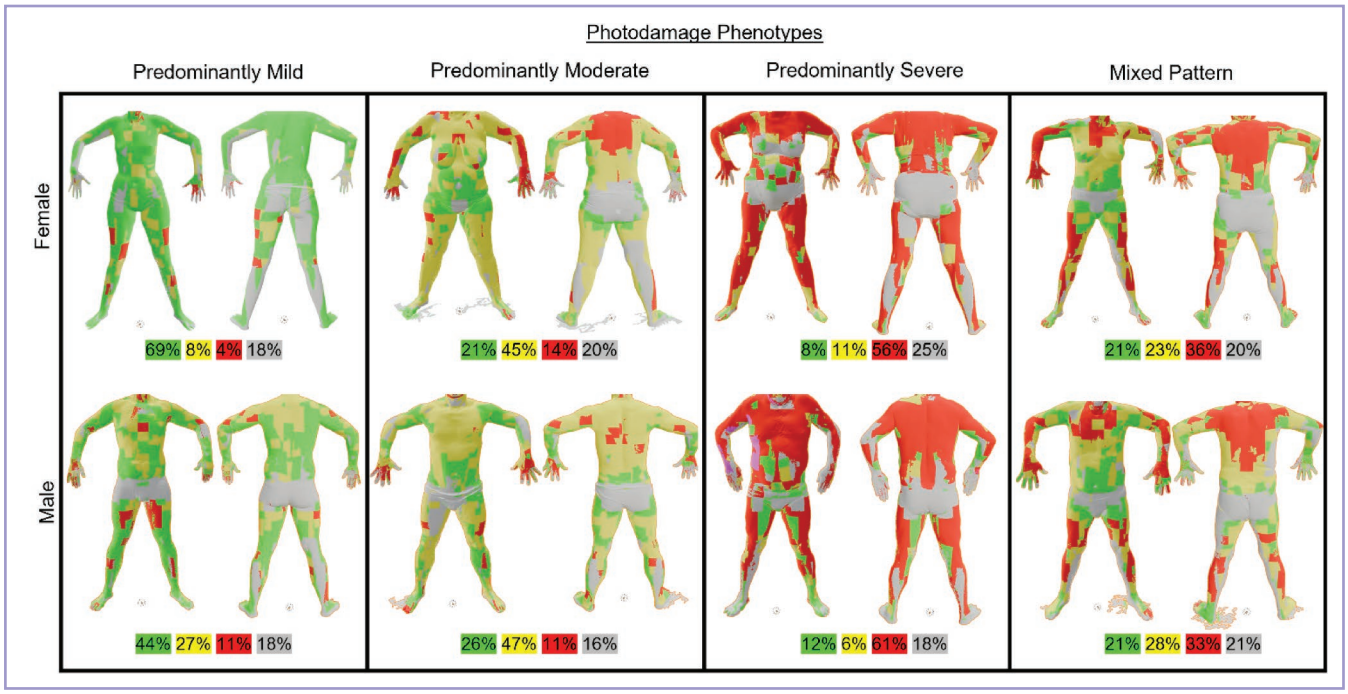

Figure 4 Photodamage heatmaps reconstructed from convolutional neural network-labelled image tiles and overlaid to three-dimensional total-body photography avatars. Surface area affected by each photodamage category was extracted and presented alongside heatmaps (green = mild; yellow = moderate; red = severe; grey = unlabelled).

test set, annotated by dermatology researchers, provided further evidence that the CNN model demonstrated excellent-to-good agreement with ground truth annotation across all body sites. In addition to demonstrating that our photonumeric scale can be effectively used for annotation in machine learning, it also holds potential for assessment of individuals in clinical or research settings.[10,29] Photonumeric scales are reported to achieve greater agreement than written instructions for dermatology clinicians and researchers, but their use has not been previously described for nondermatologist laypeople.[7] Our scale was designed for a non-expert audience, and can be applied to any body site, with high reproducibility.

Training a CNN for dermatology image classification is challenging due to the subtle and detailed variability in the appearance of the skin surface. Such tasks require an algorithm to differentiate between artificial categories (i.e. varying severities of photodamage), as opposed to classifying distinct lesion categories (i.e. melanoma).[15] The continuous fine-grained nature of photodamage is complicated by class ambiguity, where data must be segmented into standalone classes (i.e. mild) to facilitate interpretation, but the boundary between two classes lacks distinct cutoff. To address this, we employed an MTL that leveraged the (intraclass) variability of pigmentation phenotypes within a specific photodamage class. The MTL-structured CNN was designed to account for the nine distinct combinations of photodamage and pigmentation, enhancing the dimensionality of labelling for each specific image tile rather than considering photodamage in isolation.[30]

Clinical application of our photodamage CNN aims to advance the concept of precision prevention for melanoma. This concept leverages personalized risk factors, including the clinical phenotype (i.e. age, sex, family history), genotype (i.e. polygenic risk score and rare variants), and the deep imaging phenotype.[9] Deep image-based phenotyping describes the automated assessment of cutaneous risk factors (i.e. photodamage, naevi, freckling and skin colour) across the body surface area using 3D TBP and AI.[14,29,31] Among these cutaneous risk factors, ultraviolet radiation that accumulates as photodamage is the strongest environmental risk factor for melanoma, but has been excluded from risk prediction due to the challenge of site-specific assessment.[6] When incorporated into a holistic and nuanced risk assessment, precision prevention aims to stratify individuals based on personalized risk to a customized intensity and format of melanoma surveillance.[9,14] This risk stratified approach to surveillance is posited to address the limitations of underdiagnosis and overdiagnosis within existing surveillance protocols.[29,32] Specifically, the underdiagnosis of progressive melanomas may be minimized by directing high-risk individuals to intensive surveillance (i.e. clinical examination, structured surveillance using 3D TBP and sequential digital dermoscopy imaging). Conversely, overdiagnosis may be addressed by de-escalating surveillance (i.e. skin self-examinations) for individuals at low risk with indolent lesions that are unlikely to progress to metastatic melanoma.[32]

Limitations of our study were reflected in the select cohort that had largely European ancestry, a high burden of ambient UV exposure, and cutaneous malignancies. This high burden of sun exposure and skin cancers was mitigated by balanced inclusion of mild, moderate and severe photodamage phenotypes from both high- and population-risk cohorts, to prevent the CNN model from overfitting to a specific group or phenotype. Our training

dataset included images from individuals with Fitzpatrick phototypes I–III, and therefore it cannot be generalized to darker phototypes.[33,34] Photodamage assessment relied on skin photography, which is reported to have a stronger association with melanocyte TMB than histologically annotated photodamage.[35,36] However, given the method is image based rather than a calibrated quantitative modality, results may remain sensitive to pigmentation, illumination and camera differences, despite external validation. Genetic analysis was not performed to validate this directly. Prior to implementation, this algorithm should be validated in external diverse populations to calibrate the relative weightings of site-specific photodamage area and severity into a clinical risk score.[37] Our study was not powered to definitively test the association between photodamage and melanoma risk, which would require a large prospective cohort with sufficiently long follow-up to capture melanoma events.

In conclusion, we have developed and validated a photonumeric scale for assessing skin photodamage. This scale can be used in a clinical or research setting and to guide image annotation for machine learning. We then applied this scale to develop a CNN for automatic assessment of skin photodamage. Our CNN provides a novel tool to report the severity and distribution of photodamage from TBP, providing visual output that can be viewed on 3D avatars. Our CNN could be incorporated into existing or new risk-prediction models for skin cancer to assist in personalized, targeted surveillance methods for the earlier detection of melanoma.

Acknowledgements

We thank our layperson annotators and Isahit (Paris, France) for facilitating ethical access to image-labelling services. The funders had no role in the design of the study; the collection, analysis or interpretation of the data; or the writing of the manuscript; or the decision to submit it for publication.

Author contributions

Sam Kahler (Investigation, Methodology, Visualization, Writing—original draft, Writing—review & editing [equal]), Siyuan Yan (Investigation, Methodology, Visualization, Writing—review & editing [equal]), Adam Mothershaw (Investigation, Visualization, Writing—review & editing [equal]), Francesco Leo (Data curation, Investigation, Methodology, Validation [equal]), Chantal Rutjes (Investigation, Project administration, Writing—review & editing [equal]), Zhen Yu (Methodology, Supervision, Writing—review & editing [equal]), Dilki Jayasinghe (Writing—review & editing [equal]), Victoria Mar (Data curation, Project administration, Supervision, Validation [equal]), Monika Janda (Conceptualization, Funding acquisition, Project administration, Writing—review & editing [equal]), Zongyuan Ge (Funding acquisition, Methodology, Supervision, Writing—review & editing [equal]), H. Peter Soyer (Conceptualization, Funding acquisition, Methodology, Supervision, Writing—review & editing [equal]), Brigid Betz-Stablein (Conceptualization, Methodology, Supervision, Writing—review & editing [equal]) and Clare A. Primiero (Project administration, Writing—review & editing [equal]).

Funding sources

The study was funded by a National Health and Medical Research Council (NHMRC) partnership grant (1153046); NHMRC Centres of Research Excellence (grants 2006551 and 1135285); NHMRC Synergy Grant (2009923).

Conflicts of interest

H.P.S. is shareholder of e-derm consult GmbH and MoleMap by Dermatologists Pty Ltd; he provides teledermatological reports regularly for both companies; consults for Canfield Scientific Inc.; and is an adviser of First Derm. B.B.S. is an employee of Canfield Scientific Inc. The remaining authors declare no conflicts of interest.

Data availability

Anonymized photographic, annotation and participant demographic data are available on request. Images that include the head or identifying features (i.e. tattoo) have been intentionally excluded from this analysis to facilitate external validation of this work.

Ethics statement

Participants were recruited from two dermatological imaging studies conducted in Queensland, Australia, as follows: Mind Your Moles (Ethics HREC/16/QPAH/125); Health Outcomes Program Study (HREC/17/QPAH/816).

Patient consent

All patients gave written, informed consent for participation and publication of their case details and images.

Supporting Information

Additional Supporting Information may be found in the online version of this article at the publisher's website.

References

1 Arnold M, de Vries E, Whiteman DC *et al.* Global burden of cutaneous melanoma attributable to ultraviolet radiation in 2012. *Int J Cancer* 2018; **3**:1305–14.
2 Katzberg AA. The area of the dermo-epidermal junction in human skin. *Anat Rec* 1958; **131**:717–25.
3 Shain AH, Yeh I, Kovalyshyn I *et al.* The genetic evolution of melanoma from precursor lesions. *New Engl J Med* 2015; **373**:1926–36.
4 Tang J, Fewings E, Chang D *et al.* Publisher correction: The genomic landscapes of individual melanocytes from human skin. *Nature* 2021; **590**:E20.
5 Olsen CM, Neale RE, Green AC *et al.* Independent validation of six melanoma risk prediction models. *J Invest Dermatol* 2015; **135**:1377–84.
6 Kaiser I, Pfahlberg AB, Uter W *et al.* Risk prediction models for melanoma: a systematic review on the heterogeneity in model development and validation. *Int J Environ Res Public Health* 2020; **17**:7919.

7 Ayer J, Ahmed A, Duncan-Parry E *et al*. A photonumeric scale for the assessment of atrophic facial photodamage. *Br J Dermatol* 2018; **178**:1190–5.
8 McKenzie NE, Saboda K, Duckett LD *et al*. Development of a photographic scale for consistency and guidance in dermatologic assessment of forearm sun damage. *Arch Dermatol* 2011; **147**:31–6.
9 Kahler S, Rutjes C, Janda M *et al*. The deep imaging phenotype for melanoma risk stratification. *SKINdeep* 2025; **1**:e150261.
10 Usher-Smith J, Emery J, Kassianos AP, Walter FM. Risk prediction models for melanoma: a systematic review. *Cancer Epidemiol Biomarkers Prev* 2014; **23**:1450–63.
11 Garbe C, Amaral T, Peris K *et al*. European consensus-based interdisciplinary guideline for melanoma. Part 1: Diagnostics: Update 2022. *Eur J Cancer* 2022; **170**:236–55.
12 Cancer Council Australia and Melanoma Institute Australia Guidelines Working Party. Clinical practice guidelines for the diagnosis and management of melanoma. Available at: https://www.cancer.org.au/clinical-guidelines (last accessed 14 January 2026).
13 Primiero CA, Rezze GG, Caffery LJ *et al*. A narrative review: opportunities and challenges in artificial intelligence skin image analyses using total body photography. *J Invest Dermatol* 2024; **144**:P1200–7.
14 Kahler S, Primiero C, Mothershaw A *et al*. Three dimensional total body photography identifies cutaneous phenotypes associated with late-onset invasive melanoma risk. *Br J Dermatol* 2026; **194**:531–9.
15 Esteva A, Kuprel B, Novoa RA *et al*. Dermatologist-level classification of skin cancer with deep neural networks. *Nature* 2017; **542**:115–18.
16 Soenksen LR, Kassis T, Conover ST *et al*. Using deep learning for dermatologist-level detection of suspicious pigmented skin lesions from wide-field images. *Sci Transl Med* **13**:eabb3652.
17 Tschandl P, Rinner C, Apalla Z *et al*. Human–computer collaboration for skin cancer recognition. *Nat Med* **26**:1229–34.
18 Koh U, Janda M, Aitken JF *et al*. 'Mind your Moles' study: protocol of a prospective cohort study of melanocytic naevi. *BMJ Open* 2018; **8**:e025857.
19 Primiero CA, McInerney-Leo AM, Betz-Stablein B *et al*. Evaluation of the efficacy of 3D total-body photography with sequential digital dermoscopy in a high-risk melanoma cohort: protocol for a randomised controlled trial. *BMJ Open* 2019; **9**:e032969.
20 Langton KA, Ayer J, Griffiths TW *et al*. Distinctive clinical and histological characteristics of atrophic and hypertrophic facial photoageing. *J Eur Acad Dermatol Venereol* 2021; **35**:762–8.
21 He K, Zhang X, Ren S, Sun J. Deep residual learning for image recognition. *Proceedings of the IEEE Conference on Computer Vision and Pattern Recognition*, Las Vegas, 27–30 June 2016; 770–8.
22 Deng J, Dong W, Socher R *et al*. ImageNet: a large-scale hierarchical image database. *Proceedings of the IEEE Conference on Computer Vision and Pattern Recognition*, Miami, 20–25 June 2009; 248–55.
23 Yan S, Liu C, Yu Z *et al*. EPVT: Environment-aware prompt vision transformer for domain generalization in skin lesion recognition. In: *Medical Image Computing and Computer-Assisted Intervention – MICCAI 2023. Lecture Notes in Computer Science*. Cham: Springer; 249–59.
24 R Core Team (2017). *Version 3.4.1. R: A language and environment for statistical computing. The R Foundation for Statistical Computing*, Vienna, Austria, 2023.
25 Betz-Stablein B, Llewellyn S, Bearzi P *et al*. High variability in anatomic patterns of cutaneous photodamage: a population-based study. *J Eur Acad Dermatol Venereol* 2021; **35**:1896–1903.
26 Walter SD, King WD, Marrett LD. Association of cutaneous malignant melanoma with intermittent exposure to ultraviolet radiation: results of a case–control study in Ontario, Canada. *Int J Epidemiol* 1999; **28**:418–27.
27 Gordon D, Gillgren G, Eloranta S *et al*. Time trends in incidence of cutaneous melanoma by detailed anatomical location and patterns of ultraviolet radiation exposure: a retrospective population-based study. *Melanoma Res* 2015; **25**:348–56.
28 Goodman GJ, Armour KS, Kolodziejczyk JK *et al*. Comparison of self-reported signs of facial ageing among Caucasian women in Australia versus those in the USA, the UK and Canada. *Australas J Dermatol* 2018; **59**:108–17.
29 Lee KJ, Betz-Stablein B, Stark MS *et al*. The future of precision prevention for advanced melanoma. *Front Med (Lausanne)* 2022; **8**:818096.
30 Gao BB, Xing C, Xie CW *et al*. Deep label distribution learning with label ambiguity. *IEEE Transactions on Image Processing* 2017; **26**:2825–38.
31 Betz-Stablein B, D'Alessandro B, Koh U *et al*. Reproducible naevus counts using 3D total body photography and convolutional neural networks. *Dermatology* 2022; **238**:4–11.
32 Cust AE, Scolyer RA. Melanoma in situ – getting the diagnosis and prognosis right. *JAMA Dermat* 2023; **159**, 699–701.
33 Hayward NK, Wilmott JS, Waddell N *et al*. Whole-genome landscapes of major melanoma subtypes. *Nature* 2017; **545**:175–80.
34 Lopes FCPS, Sleiman MG, Sebastian K *et al*. UV exposure and the risk of cutaneous melanoma in skin of color: a systematic review. *JAMA Dermatol* 2021; **157**:213–19.
35 Baillie L, Askew D, Douglas N, Soyer HP. Strategies for assessing the degree of photodamage to skin: a systematic review of the literature. *Br J Dermatol* 2011; **165**:735–42.
36 Lee KJ, Kao YC, Smit DJ *et al*. Mitochondrial deletion^{4977} abundance in melanoma-adjacent skin. *J Invest Dermatol* 2025; **145**:1527–30.e1526.
37 Elwood JM, Jopson J. Melanoma and sun exposure: an overview of published studies. *Int J Cancer* 1997; **73**:198–203.

NO COMPROMISE, JUST CLEARANCE

Bimzelx®▼ (bimekizumab) offers the opportunity for complete, fast, and lasting skin clearance and proven PsA efficacy [1–7]

68.2% (n=238/349)

of patients with PsO achieved **PASI 100 at Week 16**

(vs 1.2% placebo [n=1/86], p<0.0001)*** [2]

75.9% (n=265/349)

of patients with PsO achieved **PASI 75 at Week 4**

(vs 1.2% placebo [n=1/86], p<0.0001)*** [2]

76.9% (N=52)†

of patients with PsO achieved **PASI 100 at 5 years**[3]

51.5% (n=222/431) and **50.6%** (n=135/267)

of biologic-naïve and TNFi-IR PsA patients achieved **ACR 50 at Week 104/100,** respectively‡ [1,4–6]

BIMZELX was well tolerated, the most frequently reported adverse reactions were: upper respiratory tract infections and oral candidiasis. Other common reported adverse reactions include tinea infections, ear infections, herpes simplex infections, oropharyngeal candidiasis, gastroenteritis, folliculitis, headache, rash, dermatitis, eczema, acne, injection site reactions, fatigue, and vulvovaginal mycotic infection (including vulvovaginal candidiasis).[4]

This promotional material has been created and funded by UCB Pharma Ltd and is intended for healthcare professionals in the UK.

BIMZELX is indicated for the treatment of: moderate to severe plaque PsO in adults who are candidates for systemic therapy; active PsA, alone or in combination with methotrexate, in adults who have had an inadequate response, or who have been intolerant, to one or more DMARDs; active nr-axSpA with objective signs of inflammation as indicated by elevated CRP and/or MRI, in adults who have responded inadequately, or are intolerant, to NSAIDs; active AS in adults who have responded inadequately or are intolerant to conventional therapy; and active moderate to severe HS (acne inversa) in adults with an inadequate response to conventional systemic HS therapy.[4]

Prescribing information for United Kingdom click here.
Please refer to the SmPC for further information.

▼This medicine is subject to additional monitoring. This will allow quick identification of new safety information. Adverse events should be reported. Reporting forms and information can be found at www.yellowcard.mhra.gov.uk for the UK. Adverse events should also be reported to UCB Pharma Ltd at UCBCares.UK@UCB.com or 0800 2793177 for UK.

These data are from different clinical trials and cannot be directly compared.

Co-primary endpoints PASI 90 and IGA 0/1 at Week 16 were met.**Secondary endpoints. †N= mNRI, missing data were imputed with mNRI (patients with missing data following treatment discontinuation due to lack of efficacy or a TRAE were counted as non-responders; multiple imputation methodology was used for other missing data). ‡43.9% (n=189/431), and 43.4% (n=116/267) of biologic-naïve and TNFi-IR PsA patients achieved the primary endpoint of ACR 50 at Week 16 in BE OPTIMAL and BE COMPLETE, respectively (vs 10.0% [n=28/281] and 6.8% [n=9/133] placebo, p<0.0001); 54.5% (n=235/431) and 51.7% (n=138/267) maintained it at Week 52 (NRI).[4–6]

ACR 50, ≥50% response in the American College of Rheumatology criteria; **AS**, ankylosing spondylitis; **CRP**, C-reactive protein; **DMARD**, disease-modifying antirheumatic drug; **HS**, hidradenitis suppurativa; **IGA**, Investigator's Global Assessment; **(m)NRI**, (modified) non-responder imputation; **MRI**, magnetic resonance imaging; **nr-axSpA**, non-radiographic axial spondyloarthritis; **NSAID**, non-steroidal anti-inflammatory drug; **PASI 75/90/100**, ≥75/90/100% improvement from baseline in Psoriasis Area and Severity Index; **PsA**, psoriatic arthritis; **PsD**, psoriatic disease; **PsO**, psoriasis; **TNFi-IR**, tumour necrosis factor-α inhibitor – inadequate responder; **TRAE**, treatment-related adverse event.

References: 1. Gordon KB, et al. Lancet. 2021;397(10273):475–486. 2. Blauvelt. 2025. AAD Presentation 62275. 3. Mease PJ, et al. Rheumatol Ther. 2024;11(5):1363–1382. 4. BIMZELX SmPC. 5. Ritchlin CT, et al. Ann Rheum Dis. 2023;82(11):1404–1414. 6. Coates LC, et al. RMD Open. 2024;10(1):e003855. 7. Strober B, et al. AAD 2024;oral presentation.

Inspired by patients. Driven by science.

GB-BK-2500315 | July 2025

Bimzelx®▼ (bimekizumab)